Unsteady Boundary-Layer Flow over an Oscillating Thin Foil

WEN-HWA CHU*
Southwest Research Institute, San Antonio, Texas

In this study, the unsteady potential flow at the edge of the boundary layer over a pitching and heaving foil was derived first. The harmonic components of the unsteady boundary layer were then calculated, based on a new approximation analogous to an Oseen-type equation, as an extension to the diffusion equation used by C. C. Lin for rapidly oscillating streams. The mean boundary-layer flow with effective pressure gradient terms was subsequently calculated by the Karman-Pohlhausen method and numerical integration, and the point of instability was determined by the use of the universal stability curve. However, nowhere on the foil did the minimum wall shear vanish. A tentative explanation of the discrepancy between the theory and some experiments is given. Considerably more work remains to be done for better understanding of the title problem.

Nomenclature

a = velocity profile parameter; see Eq. (30)
a_E = location of elastic axis aft midchord point
A_n = coefficients in the Glauert-type series
b = semichord
bl = boundary layer
c = chord length
$C(k)$ = Theodorsen function, Eq. (15a)
$D(k)$ = defined by Eq. (15b)
h = heaving displacement, positive upward
$\dot{h}$ = heaving velocity
$H_1^{(2)}(k)$, $H_0^{(2)}(k)$ = Hankel's function of the 2nd kind of order 1 and 0, respectively
i = $(-1)^{1/2}$
$\mathbf{i}, \mathbf{j}, \mathbf{k}$ = unit vector along x, y
k = reduced frequency based on semichord, $\omega b/U_\infty$
k_c = reduced frequency based on chord, $\omega c/U_\infty$
K = second shape parameter; see Eq. (39)
p = pressure
$\tilde{p}$ = effective pressure
$\bar{p}$ = mean effective pressure
p' = perturbed effective pressure
$\mathbf{q}$ = velocity vector in foil fixed coordinates
Q = the effective pressure gradient
$\mathbf{r}$ = position vector
R = Reynolds number base on semichord, $U_\infty c/2\nu$
R_δ = Reynolds number base on the displacement thickness, $U_\infty \delta_*/\nu$ or $2R\delta_*$*
r_0 = leading-edge radius of curvature
t = time
$\tilde{u}$ $\tilde{v}$ = average x and y component of velocity in the bl, respectively
u_1, v_1 = perturbed x and y component of velocity in the bl, respectively
U_s, U_c = amplitude of the sine and cosine components of U_1, respectively
u_s, u_c = amplitude of the sine and cosine components of u, inside the bl
U_p, σ = amplitude and phase angle of U_1; see Eq. (27)
u_0 = x component of the mean velocity in the bl
U_∞ = velocity at upstream infinity
$U_0(x)$ = mean velocity at $y = \delta$
$U_1(x,t)$ = unsteady perturbation at $y = \delta$
u, v, w = velocity components in x, y, and z directions, respectively
$\tilde{v}_0$, $\tilde{v}_1$ = nondimensional velocity at midchord and $\frac{3}{4}$-chord, respectively
x, y, z = Cartesian coordinates (foil-fixed)
z^* = see Eq. (41)
α = wave number
α_0 = amplitude of pitching oscillation, positive nose up
$\tilde{\gamma}$ = strength of the vortex sheet
δ = boundary-layer thickness or a number $\ll 1$
δ_* = displacement thickness
δ_{0n} = Kronecker delta
ϵ = symmetrical Joukowski's profile parameter [circle plane radius $(1 + \epsilon)b$]; in Figs. 1a and 1b, ϵ is the distance of the elastic axis ahead of the $\frac{1}{4}$-chord point
θ = momentum thickness
κ = velocity profile parameter
Λ_E = effective shape parameter; see Eq. (31)
ν = kinematic viscosity
ρ = density
τ_0 = shearing stress at the wall
ϕ = an angle defined by Eq. (13a)
ω = frequency of oscillation
Ω = angular velocity vector of the foil
D/Dt = Stokes' derivative

Superscripts and subscripts

$(\dot{})$ = time derivative of ( )
$(\ )^*$ = ( ) is nondimensionalized; see Eq. (26)
$(\bar{\ })$ = ( ) is an average
I = in inertia frame
F = in foil fixed frame

Introduction

THE prediction of hydrofoil flutter is a problem of practical interest[1] as there is a flutter boundary in the low mass-density region near which the existing theories fail to be conservative.[2] In fact, flutter (subcavitating) is possible[3] in the predicted flutter-free zone. Since the cause of this discrepancy is believed to be hydrodynamic in origin,[2] a critical re-evaluation of theory and experiments was conducted by Ref. 4. In Ref. 5, it was found that some serious discrepancies between aerodynamic theory and experiments were first observed and then practically eliminated by the introduction of a disturbance wire. The cause of these discrepancies was at

Received August 25, 1967; revision received November 27, 1967. The research presented was supported by the internal research program of the Southwest Research Institute. The author would like to thank R. Gonzales for his efforts in the computer programming.

* Senior Research Engineer, Department of Mechanical Sciences. Member AIAA.

tributed to the oscillation of the transition point in the aft part of the foil. However, it was uncertain whether oscillation of the separation point existed before the trailing edge; hence, the flowfield deviates from the classical vortex sheet model. The object of the present study, therefore, is to predict the transition and the separation of the unsteady boundary layer over an oscillating foil.

On the other hand, the unsteady boundary-layer flow was a subject of research even before the invention of the hydrofoil boat. In Ref. 6, for example, a series expansion in derivations of the unsteady freestream was proposed, and, in Ref. 7, other mathematical methods were considered, such as 1) iteration on the differential equation and 2) linearization of oscillation (C. C. Lin method[8]). Series solution is also used in Ref. 7, but with an expansion in terms of the relative amplitude of oscillation. Since the basic potential flow employed in the present paper is much more complex, a new approximation analogous to Oseen's equation will be used. Here note that an unsteady Oseen's flow over an oscillative foil was investigated in Refs. 9 and 10†; other unsteady laminar boundary-layer theories were reviewed in Ref. 11.

Formulation of Problem

In foil-fixed coordinates, the equation of motion for incompressible viscous flow takes the form

$$D\mathbf{q}/Dt = -(1/\rho)\nabla p + \nu\nabla^2\mathbf{q} - 2(\boldsymbol{\Omega}\times\mathbf{q}) - (\boldsymbol{\Omega}\times\boldsymbol{\Omega}\times\mathbf{r}) - \dot{\boldsymbol{\Omega}}\times\mathbf{r} \quad (1)$$

$$= -(1/\rho)\nabla\tilde{p} + \nu\nabla^2\mathbf{q} - 2(\boldsymbol{\Omega}\times\mathbf{q}) + (\boldsymbol{\Omega}\times\boldsymbol{\Omega}\times\mathbf{r}) - 2\mathbf{i}y\ddot{\alpha} + \mathbf{j}2\dot{\alpha}U_\infty \quad (1a)$$

where

$$\boldsymbol{\Omega} = -\dot{\alpha}\mathbf{k} = 0(\delta) \quad (1b)$$

$$\tilde{p} = p - \ddot{\alpha}xy - 2\dot{\alpha}U_\infty y \quad (1c)$$

Assume that the outer potential flow is known in space-fixed coordinates (inertia frame) and is slightly perturbed by the thin foil. Then,

$$\mathbf{q}_I = \mathbf{q} + \boldsymbol{\Omega}\times[\mathbf{r} - (b + a_E)] \quad (2)$$

At infinity,

$$\mathbf{q}_I \to U_\infty \quad (3a)$$

$$\mathbf{q} \to U_\infty + \mathbf{i}(-\dot{\alpha}y) + \mathbf{j}\dot{\alpha}[x - (b + a_E)] - \mathbf{j}\dot{h} \quad (3b)$$

At $y = \delta$,

$$\mathbf{q}_I \to \mathbf{j}\{-\dot{\alpha}[x - (b + a_E)]\} + \dot{h}\mathbf{j} + \mathbf{i}U(x,t) \quad (4a)$$

$$\mathbf{q} \to \mathbf{i}\{U_0(x) + U_1(x,t)\} \quad (4b)$$

$$\Delta\tilde{p}/\partial x \to \partial p/\partial x \quad (4c)$$

At $y = 0$,

$$\mathbf{q} \to 0 \quad (5)$$

For small periodic oscillations of thin air foils,

$$U(x,t) \cong U_\infty + U_s\sin(\omega t) + U_c\cos(\omega t) \quad (6)$$

which will be given later.

† In Ref. 9, the number n_R, in Eq. (76), does not have to be the number n_R as in Eq. (69a, b) which validates Eqs. (71) and (72) for all n. Thus, n_R can be set to infinity in Eq. (76) leading to a finite limit. Based on Oseen's equation, both Refs. 9 and 10 reached the conclusion that the trailing-edge singularity is of the order of the logarithm of the Reynolds number divided by Reynolds number, which is negligible for the large Reynolds number considered.

In the neighborhood of the body, Eq. (1a) reduces approximately to the boundary-layer equations,

$$\partial u/\partial t + u\,\partial u/\partial x + v\,\partial u/\partial y = -(1/\rho)(\partial\tilde{p}/\partial x) + \nu\,\partial^2 u/\partial y^2 \quad (7a)$$

$$\partial u/\partial x + \partial v/\partial y = 0 \quad (7b)$$

$$\partial\tilde{p}/\partial y = 0(\delta) \quad (7c)$$

At $y = \delta$,

$$\tilde{p} = \tilde{p} + p' \qquad u = U_0(x) + U_1(x,t)$$
$$-(1/\rho)(\partial\tilde{p}/\partial x) = (\partial U/\partial t) + U(\partial U/\partial x) \quad (8a)$$

$$-(1/\rho)(\partial\tilde{p}/\partial x) = \overline{U_1\,\partial U_1/\partial x} + U_0\,\partial U_0/\partial x \quad (8b)$$

$$-\frac{1}{\rho}\frac{\partial p'}{\partial x} = \frac{\partial U_1}{\partial t} + U_0\frac{\partial U_1}{\partial x} + U_1\frac{\partial U_0}{\partial x} + U_1\frac{\partial U_1}{\partial x} - \overline{U_1\frac{\partial U_1}{\partial x}} \quad (8c)$$

Let $u = \bar{u} + u_1(x,t)$, $v = \bar{v} + v_1(x,t)$ inside the boundary layer.

The well-known equations in the Lin method[12] follow‡:

$$\partial\bar{u}/\partial x + \partial\bar{v}/\partial y = 0 \quad (9a)$$

$$\partial u_1/\partial x + \partial v_1/\partial y = 0 \quad (9b)$$

$$\bar{u}\,\partial\bar{u}/\partial x + \bar{v}\,\partial\bar{u}/\partial y = \nu\,\partial^2\bar{u}/\partial y^2 + U_0\,\partial U_0/\partial x + Q \quad (10)$$

$$Q = U_1\,\Delta U_1/\partial x - \overline{u_1\,\partial u_1/\partial x} - \overline{v_1\,\partial u_1/\partial y} \quad (10a)$$

$$\frac{\partial u_1}{\partial t} + \bar{u}\frac{\partial U_1}{\partial x} = \nu\frac{\partial^2 u_1}{\partial y^2} + \frac{\partial U_1}{\partial t} + U_0\frac{\partial U_1}{\partial x} + E \quad (11)$$

$$E = E_1 + E_2 \quad (12)$$

where

$$E_1 = \bar{u}\frac{\partial}{\partial x}(U_1 - u_1) - u_1\frac{\partial\bar{u}}{\partial x} - v_1\frac{\partial\bar{u}}{\partial y} - \bar{v}\frac{\partial u_1}{\partial y} + U_1\frac{\partial U_0}{\partial x} \quad (12a)$$

$$E_2 = -u_1\frac{\partial U_1}{\partial x} - v_1\frac{\partial u_1}{\partial y} + \overline{u_1\frac{\partial u_1}{\partial x}} + \overline{v_1\frac{\partial u_1}{\partial y}} + U_1\frac{\partial U_1}{\partial x} - \overline{U_1\frac{\partial U_1}{\partial x}} \quad (12b)$$

For small, unsteady, sinusoidal perturbations, each term of E_1 is of the order of δ^2, or smaller, at the edge of the boundary layer and at the foil. This is so because $\partial u_1/\partial x - \partial U_1/\partial x = 0$ at the edge of the boundary layer, and $\bar{u} = 0$ at the foil; $u_1 = O(\delta)$, $[\partial u/\partial x \le O(\delta)]$ at the edge of the boundary layer, and $u_1 = 0$ at the foil; $\partial\bar{u}/\partial y = \partial\bar{v}/\partial x = O(\delta)$, $v_1 = O(\delta)$ at the edge of the boundary layer, and $v_1 = 0$ at the foil; $\partial u_1/\partial y = \partial v_1/\partial x = O(\delta)$, $\bar{v} = O(\delta)$ at the edge of the boundary layer, and $\bar{v} = 0$ at the foil; $u_1 = O(\delta)$, $\partial U_0/\partial x = 0$ at the edge of the boundary layer, $U_1 = 0$, and $\partial U_0/\partial x \le O(\delta)$ on the foil. Therefore, the products in E_1 and thus E_2 are assumed to be negligible. For harmonic oscillations, E_2 are contributions of second harmonics and constants, thus, will not be included. Also, the effect of 2nd and higher harmonics on the mean motion will be assumed negligible. Equation (11), with $E = 0$, is regarded as an improvement of the diffusion equation used by Lin, since the assumption of a high reduced frequency is removed. However, the order-of-magnitude assumption is now imposed. Consequently, the accuracy of this approximation remains to be examined by experiment.

‡ The same set of equations can be derived by balancing the harmonic part and constant part separately.

Unsteady Potential Flow

There is a leading-edge singularity of the unsteady potential flow for thin airfoils. This may accentuate the leading-edge singularity in the boundary-layer flow. Therefore, the potential flow singularity will be removed by considering a slightly rounded leading edge. In this study, the foil is assumed to be symmetrical and approximated by a symmetrical Joukowski's airfoil with the same leading-edge curvature. Assuming that the circle plane potential is given by the Glauert series and neglecting the higher-order terms in the scale factor of mapping, one finds, with Kutta's condition, that

$$\frac{\gamma(x')}{U_\infty} = \frac{2U_1(x)}{U_\infty} = 2\left[A_0(1-\cos\phi) + \sum_{n=1}^{\infty} A_n \sin(n\phi)\sin\phi\right]\frac{1}{[\sin^2\phi + \epsilon^2(1-\cos\phi)^2]^{1/2}} \quad (13)$$

which reduces to the well-known Glauert series for ϵ identical to 0. In Eq. (13),

$$\phi = \cos^{-1}(2x-1) \quad (13a)$$

The well-known governing integral equation (cf. Ref. 14, p. 275) for pitching and heaving is

$$-\frac{1}{2\pi}\int_{-1}^{1}\frac{\gamma(x_1)dx_1}{x'-x_1} = U_\infty[\bar{v}_0 - 2(\bar{v}_0-\bar{v}_1)x'] - \frac{\tilde{k}\Gamma}{2\pi}e^{ik}\int_{1^+}^{\infty}\frac{e^{-ikx_1}}{x'-x_1}dx_1 \quad (14)$$

In this equation, $x' = -\cos\phi'$ is measured from the midchord point and nondimensionalized by the semichord b, whereas in this paper, x is measured from the leading edge and nondimensionalized by the chord c. Therefore,

$$2x - 1 = -\cos\phi' = x' \quad (14a)$$

$$\phi' = \pi - \phi \quad (14b)$$

The Glauert method, with $\epsilon = 0$, yields[13]

$$A_n = (-1)^{n-1}B_n \quad (15)$$

$$B_n = +\frac{ik\tilde{\Gamma}e^{ik}}{2\pi(1+\delta_{0n})}\frac{2}{\pi}\int_0^{\pi}\int_1^{\infty}\frac{e^{-ikx_1}\cos(n\phi')dx_1}{\cos\phi' + x_1}d\phi' - \delta_{n0}\bar{v}_0 + 2\delta_{n1}(\bar{v}_0-\bar{v}_1) \quad (15a)$$

where

$$\tilde{\Gamma} = 2\pi U[A_0 + A_1/2] = 2\pi U D(k)\bar{v}_1 \quad (15b)$$

By using a recurrence relation and solving the resultant difference equation, one finds

$$I_n = +\frac{1}{\pi}\int_0^{\pi}\frac{\cos(n\phi')}{\cos\phi' + \cosh\phi_1}d\phi' = e^{-n\phi_1}(-1)^n \quad (16a)$$

$$x_1 = \cosh\phi_1$$

and

$$A_n = -2\bar{v}_1 \cdot ike^{ik}\,D(k)S_n(k) - \delta_{n0}\bar{v}_0 + 2\delta_{n1}(\bar{v}_0-\bar{v}_1) \quad (16b)$$

where

$$S_n(k) = \int_0^{\infty} e^{-ik\cos\phi - n\phi}d\phi \quad (16c)$$

which can be evaluated numerically. It is also possible to express A_n in Bessel functions, but the effort increases as n increases. Only the first four coefficients have been expressed explicitly in closed form as follows:

$$A_0 = \{-\bar{v}_0 + [1-C(k)]\bar{v}_1\} \quad (17a)$$

$$A_1 = +2\{(\bar{v}_0-\bar{v}_1) + \bar{v}_1[D(k)+C(k)]\} \quad (17b)$$

$$A_2 = -\bar{v}_1\left\{\left(-4-\frac{4}{ik}\right)D(k) - \frac{4}{ik}C(k) - 2[1-C(k)]\right\} \quad (17c)$$

$$A_3 = \bar{v}_1\left\{\left(6+\frac{16}{ik}-\frac{16}{k^2}\right)D(k) + \left(2-\frac{16}{k^2}\right)C(k) + \frac{8}{ik}[1-C(k)]\right\} \quad (17d)$$

$$A_4 = -\bar{v}_1\left\{\left(-8-\frac{40}{ik}+\frac{96}{k^2}+\frac{96}{ik^2}\right)D(k) + \left(\frac{96}{ik^3}-\frac{16}{ik}\right)C(k) - \left(2-\frac{48}{k^2}\right)[1-C(k)]\right\} \quad (17e)$$

where

$$C(k) = \frac{H_1^{(2)}(k)}{H_1^{(2)}(k) + iH_0^{(2)}(k)} \quad \text{Theodorsen function} \quad (18a)$$

$$D(k) = \{[\pi/2)ike^{ik}[H_1^{(2)}(k) + iH_0^{(2)}(k)]\}^{-1} \quad (18b)$$

$$\bar{v}_1 = ik(h_0/b) - \alpha_0 + ik(a_E/b - \tfrac{1}{2})\alpha_0 \quad (18c)$$

$$\bar{v}_0 - \bar{v}_1 = (ik/2)\phi_0 \quad (18d)$$

It is noted that the expression $A_n(k)$ for $n \geq 1$ differs from those in Ref. 13 by a factor $(-1)^n$, since θ inRef. 13 was replaced by $\pi - \phi$ (where $x = -\cos\theta$ with the origin of the coordinates at midchord in Ref. 13).

For $n > 4$, $S_n(k)$ are evaluated numerically. However, the Glauert series is not term by term twice differentiable. Therefore, Eq. (16) is integrated by parts;

$$S_n = e^{-ik}/n - (ike^{-ik}/n^3) + R_n \quad (19)$$

$$R_n = 0(1/n^4) \quad (19a)$$

R_n will be neglected for large n, say $n \geq 11$.

Summing up the tail of the series, one finds for $e^{i\omega t}$ motion,

$$U_I^* = U_I + U_{II} + U_{III} \quad (20)$$

$$U_I = \sum_{n=1}^{N}\bar{A}_n \sin(n\phi)\frac{\sin\phi}{[\sin^2\phi + \epsilon^2(1-\cos\phi)^2]^{1/2}} + \frac{A_0(1-\cos\phi)}{[\sin^2\phi + \epsilon^2(1-\cos\phi)^2]^{1/2}} \quad (21)$$

where

$$\bar{A}_n = A_n - [(-2v_1)/n]\,ikD(k) - [(-2v_1)/n^3]k^2D(k) \quad (21a)$$

$$n = 1\text{–}4$$

$$\bar{A}_n = [S_n(k) - (1/n)e^{-ik} + (ike^{-ik}/n^3)](-2v_1)ike^{ik}D(k) \quad (21b)$$

$$n = 5\text{–}N$$

$$U_{II} = (-2v_1)ikD(k)\cdot\frac{1}{\pi}(\pi-\phi)\frac{\sin\phi}{[\sin^2\phi + \epsilon^2(1-\cos\phi)^2]^{1/2}} \quad (22a)$$

$$U_{III} = (-2v_1)k^2D(k)\frac{1}{6\pi}[(\pi-\phi)^3 - \pi^2(\pi-\phi)]\frac{\sin\phi}{[\sin^2\phi + \epsilon^2(1-\cos\phi)^2]^{1/2}} \quad (22b)$$

The following Fourier expansions with $0 \leq \phi \leq \pi$ are used:

$$\sum_{n=1}^{\infty}\frac{1}{n}\sin(n\phi) = \frac{1}{\pi}(\pi-\phi) \quad (23a)$$

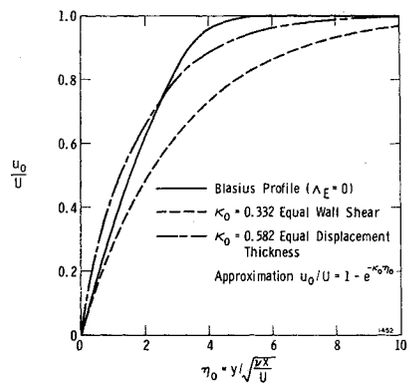

Fig. 1 An example of the approximate and exact velocity profiles.

$$\sum_{n=1}^{\infty} \frac{1}{n^3} \sin(n\phi) = \frac{1}{6\pi} [(\pi - \phi)^3 - \pi^2(\pi - \phi)] \quad (23b)$$

Equation (20) can be differentiated without difficulty to get the first and second derivatives of U_I, and superpositions can be made for real sinusoidal motion.

It is noted that the relation between leading-edge radius and ϵ is

$$r_0/c \cong 4\epsilon^2 \quad (24)$$

Unsteady Boundary-Layer Flow

Equation (11) in conjunction with Eq. (20) yields the new approximation

$$\frac{\partial u_1}{\partial t} + u_0 \frac{\partial U_1}{\partial x} = \nu \frac{\partial^2 u_1}{\partial y^2} + \frac{\partial U_1}{\partial t} + U_0 \frac{\partial U_1}{\partial x} \quad (25)$$

Let

$$x^* = x/c \qquad y^* = y/c \qquad k_c = \omega c/U_0$$
$$\delta^* = \delta/c \qquad R = U_\infty c/2\nu \quad (26)$$
$$u^* = u/U_\infty \qquad v^* = v/U_\infty$$

For oscillating thin airfoils, assume

$$U_0 \cong U_\infty \qquad U_1 = U_p(x) \sin[\omega t + \sigma(x)] \quad (27)$$

$$u_1 = u_s(x,y) \sin(\omega t + \sigma) + u_c(x,y) \cos(\omega t + \sigma) \quad (28)$$

Assuming U_p and $d\sigma/dx^*$ are both of $O(\delta)$, so that their product can be neglected, Eq. (25) yields§

$$k_c u_s^* \cong (1/2R)(\partial^2 u_c^*/\partial y^{*2}) + k_c U_p^* \quad (29a)$$

$$-k_c u_c^* + u_0^* \partial U_p^*/\partial x^* = (1/2R)(\partial^2 u_s/\partial y^{*2}) + \partial U_p^*/\partial x^* \quad (29b)$$

Further, for approximate purposes, the mean boundary-layer velocity profile is represented by an exponential function with the same displacement thickness; i.e.,

$$u_0^* = 1 - e^{-\kappa\eta} = 1 - e^{-ay^*} \quad (30)$$

where

$$a = [(\kappa/\gamma_0)(2R)^{1/2}]/(x^*)^{1/2} \quad (30a)$$

$$\delta = \gamma_0(\nu x/U)^{1/2} \qquad \gamma_0 \cong 5.733 \quad (30b)\P$$

For the Blasius profile, $\kappa_0 \cong 0.582$ (Fig. 1), $\kappa = \gamma\kappa_0 \cong 3.34$.

§ U_p is of $O(\delta)$ (except in the vicinity of the leading edge). The same assumption has been made in classical unsteady flow theory.

¶ $(\delta_*)_{\text{Blasius}} = 1.72(\nu x/U_\infty)^{1/2} = (\delta_*)_{\Lambda_E=0} = 0.3\gamma(\nu x/U_\infty)^{1/2}$ which determines γ.

Since the velocity profile varies with the distance x, the Karman-Pohlhausen method will be used in which the velocity profile is represented by a fourth-degree polynomial;

$$u_0/U_0 = a_L\eta + b_L\eta^2 + c_L\eta^3 + d_L\eta^4 \quad (31)$$

where

$$a_L = 2 + \tfrac{1}{6}\Lambda_E \quad (31a)$$
$$b_L = -\Lambda_E/2 \quad (31b)$$
$$c_L = -2 + \Lambda_E/2 \quad (31c)$$
$$d_L = 1 - \Lambda_E/6 \quad (31d)$$

For equal displacement thickness,

$$\kappa = 120/(36 + \Lambda_E) \quad (32)$$

where $\Lambda = 0$, $\kappa \cong 3.34$. With Eq. (30), the unsteady boundary-layer velocity can be integrated readily from Eqs (29a) and (29b), and one finds

$$u_s^* = u_s^{(0)} + u_s^{(1)} \qquad u_c^* = u_c^{(0)} + u_c^{(1)} \quad (33)$$

where

$$u_s^{(0)} = U_p^*[1 - e^{-\lambda y^*} \cos(\lambda y^*)] \quad (34a)$$
$$u_c^{(0)} = U_p^* e^{-\lambda y^*} \sin(\lambda y^*) \quad (34b)$$
$$\lambda = (k_c R)^{1/2} \quad (34c)$$

$$u_s^{(1)} = \{\alpha_{21}[-e^{-ay^*} + e^{-\lambda y^*} \cos(\lambda y^*)] + \alpha_{11} e^{-\lambda y^*} \sin(\lambda y^*)\}(1/k_c)(\partial U_p^*/\partial x^*) \quad (35a)$$

$$u_c^{(1)} = \{\alpha_{11}[-e^{-ay^*} + e^{-\lambda y^*} \cos(\lambda y^*)] - \alpha_{21} e^{-\lambda y^*} \sin(\lambda y^*)\}(1/k_c)(\partial U_p^*/\partial x^*) \quad (35b)$$

$$\alpha_{21} = \frac{a^2/2\lambda^2}{1 + a^4/4\lambda^4} \quad (35c)$$

$$\alpha_{11} = \frac{1}{1 + a^4/4\lambda^4} \quad (35d)$$

The velocity components with superscript 0 are those corresponding to Lin's solution[12] for a rapidly oscillating stream. The velocity components with superscript 1 represents the present corrections to Lin's solution.

With Eqs. (33–35) and Eq. (9b), one can express Q^*, Q_0 and I in closed form;

$$Q^* = Qb/U_\infty^2 = \overline{U_1^* \partial U_1^*/\partial x^*} - \overline{u_1^* \partial u_1^*/\partial x^*} - \overline{v_1^* \partial u_1^*/\partial y^*} \quad (36a)$$

$$\cong Q_0 - \frac{1}{2}\left[u_s \frac{\partial u_s}{\partial x} + u_c \frac{\partial u_c}{\partial x}\right] - \frac{1}{2}\left[v_s \frac{\partial u_s}{\partial y} - v_c \frac{\partial v_c}{\partial y}\right]$$

$$Q_0 = \tfrac{1}{2} U_s^*(\partial U_s^*/\partial x^*) + \tfrac{1}{2} U_c^* \partial U_c^*/\partial x^* \quad (36b)$$

$$I(x^*) = \int_0^\infty Q^* dy^* \quad (36c)$$

Because of limited space, the lengthy expressions of these quantities are omitted here.

Mean (Laminar) Boundary-Layer Flow

The mean boundary-layer flow is governed by Eqs. (9a) and (10). It will be determined approximately by the well-known Karman-Pohlhausen method.[12] The modified momentum integral equation states

$$(d/dx^*)(U_0^{*2}\theta^*) + \delta_*^* U_0^*(dU_0^*/dx^*) + I(x^*) = \tau_0^* \cong (1/2R)(\partial u^*/\partial y^*)_{y^*=0} \quad (37)$$

As mentioned in the previous section, a fourth-degree poly-

Table 1 Effect of the parameter ϵ on unsteady velocity distribution

($k = 0.25$, $R = 1.5 \times 10^5$, $\alpha_0 = 0.95°$, $a_E = -0.5453b$)

	$\epsilon = 0.0418$		$\epsilon = 0.020$		$\epsilon = 0.060$	
x	U_s	U_c	U_s	U_c	U_s	U_c
0.01	0.2260	−0.03800	0.2401	−0.0404	0.2102	−0.03534
0.05	0.10607	−0.01519	0.1074	−0.01538	0.1043	−0.01494
0.10	0.0741	−0.00836	0.07457	−0.00841	0.07352	−0.00829
0.20	0.05028	−0.00275	0.0504	−0.00276	0.5009	−0.00274
0.30	0.03895	-4×10^{-5}	0.0390	-4.09×10^{-5}	0.03886	-4.05×10^{-5}
0.40	0.03163	0.00150	0.03166	0.00150	0.03159	0.00150
0.50	0.02613	0.00233	0.02614	0.00233	0.02611	0.00232
0.60	0.02155	0.00256	0.02156	0.00260	0.02154	0.00259
0.70	0.01741	0.00235	0.01741	0.00235	0.01740	0.00235
0.80	0.01331	0.00152	0.01331	0.001519	0.01330	0.00158
0.90	0.00869	-1.5×10^{-4}	0.00869	-1.56×10^{-4}	0.00869	-1.56×10^{-4}
0.95	0.00570	−0.00165	0.00570	−0.00162	0.00570	−0.00162
0.99	0.00189	−0.00381	0.00186	−0.00381	0.00186	−0.00381

($k = 1.0$, $R = 1.5 \times 10^{-5}$, $\alpha_0 = 0.95°$, $a_E = -0.5453$)

	$\epsilon = 0.0418$		$\epsilon = 0.20$		$\epsilon = 0.60$	
x	U_s^*	U_c^*	U_s^*	U_c^*	U_s^*	U_c^*
0.01	0.2026	−0.003415	0.2152	−0.00363	0.1884	−0.00318
0.05	0.1066	0.01274	0.1079	0.01290	0.1048	0.0125
0.10	0.08455	0.02130	0.08506	0.02142	0.0839	0.02113
0.20	0.07126	0.03096	0.07145	0.03104	0.07100	0.03085
0.30	0.06625	0.03644	0.06635	0.03649	0.06611	0.03636
0.40	0.06309	0.03939	0.06316	0.03943	0.0630	0.03934
0.50	0.06015	0.04029	0.06019	0.04032	0.06010	0.04025
0.60	0.05668	0.03921	0.05671	0.03923	0.05665	0.03919
0.70	0.05207	0.03591	0.05208	0.03593	0.05205	0.03590
0.80	0.04548	0.02965	0.04549	0.02966	0.04547	0.02964
0.90	0.03505	0.01842	0.03505	0.01842	0.03505	0.01841
0.99	0.01378	−0.00587	0.01378	−0.00587	0.01378	−0.00587

nomial is employed with the shape factor

$$\Lambda_E = -\left[\frac{\partial^2(u_0/U_0)}{\partial\eta^2}\right]_{\eta=0} \tag{38}$$

The second shape factor is modified to

$$K = 2R\theta^{*2}[dU_0^*/dx^* + Q_0^*/U_0^*] = \Lambda_E(\theta^*/\delta^*)^2 \tag{39}$$

Replacing the known shape factor[12] Λ by Λ_E, one has

$$\delta_*^*/\delta^* = \tfrac{3}{10} - \tfrac{1}{120}\Lambda_E \tag{40a}$$

$$\theta^*/\delta^* = \tfrac{37}{315} - \tfrac{1}{945}\Lambda_E - \tfrac{1}{90720}\Lambda_E^2 \tag{40b}$$

$$2R\tau_0\delta = (2 + \tfrac{1}{6}\Lambda_E)U_0 = (\partial u/\partial\eta)_{\eta=0} \tag{40c}$$

Let

$$z^* \equiv 2R\theta^2 \tag{41}$$

The problem can be solved numerically from the following two simultaneous equations:

$$dz^*/dx^* = (2/U_0^*)\{f_2(\Lambda_E) - 2[2 + f_1(\Lambda_E)] \times z^*(dU_0^*/dx^*)\} - [2(2R)^{1/2}/U_0^{*2}]z^{*1/2}I(x^*) \tag{42a}$$

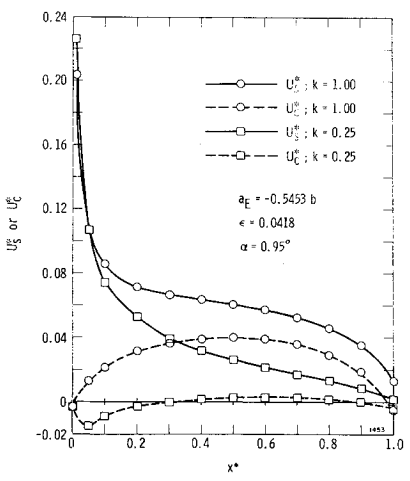

Fig. 2 Amplitudes of sine and cosine component of the unsteady perturbation velocity at the edge of the boundary layer.

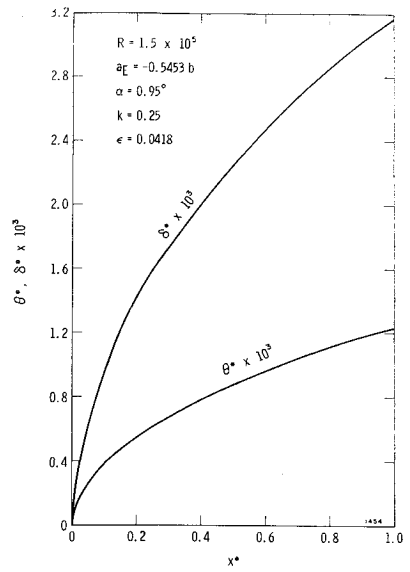

Fig. 3 Boundary-layer thickness of the mean boundary layer.

Table 2 Effect of the amplitude of oscillation on the mean boundary-layer characteristics

		($R = 1.5 \times 10^5$, $k = 0.25$, $a_E = -0.5453$)						
		$\alpha_0 = 0°$, $\epsilon = 0.0418$			$\alpha_0 = 0.95°$, $\epsilon = 0.0418$			
x	Λ_E	θ^*	R_δ	$\delta_*{}^*$	Δ_E	θ^*	R_δ	$\delta_*{}^*$
0								
0.01	0	1.25×10^{-4}	95.9	3.19×10^{-4}	−0.1689	1.06×10^{-4}	82.1	$2.736 \times 10^{-}$
0.10	0	3.96×10^{-4}	303.2	1.001×10^{-3}	−0.1481	3.81×10^{-4}	292.7	$9.758 \times 10^{-}$
0.20	0	5.60×10^{-4}	428.8	1.429×10^{-3}	−0.1497	5.48×10^{-4}	421.2	$1.424 \times 10^{-}$
0.30	0	6.85×10^{-4}	525.2	1.751×10^{-3}	−0.1503	6.76×10^{-4}	519.1	$1.730 \times 10^{-}$
0.40	0	7.91×10^{-4}	606.5	2.022×10^{-3}	−0.1507	7.82×10^{-4}	601.3[a]	$2.004 \times 10^{-}$
0.50	0	8.85×10^{-4}	687.0[a]	2.26×10^{-3}	−0.1509	8.77×10^{-4}	673.6	$2.245 \times 10^{-}$
0.60	0	9.69×10^{-4}	742.7	2.476×10^{-3}	−0.1510	9.62×10^{-4}	738.9	$2.463 \times 10^{-}$
0.70	0	1.047×10^{-3}	802.3	2.674×10^{-3}	−0.1510	1.040×10^{-3}	798.8	$2.663 \times 10^{-}$
0.80	0	1.119×10^{-3}	857.7	2.859×10^{-3}	−0.1507	1.112×10^{-3}	854.5	$2.843 \times 10^{-}$
0.90	0	1.187×10^{-3}	909.8	3.032×10^{-3}	−0.1496	1.180×10^{-3}	906.7	$3.022 \times 10^{-}$
0.99	0	1.245×10^{-3}	954.1	3.180×10^{-3}	−0.1445	1.236×10^{-3}	949.9	$3.166 \times 10^{-}$
x		$\alpha_0 = 3°$, $\epsilon = 0.0418$				$\alpha_0 = 5°$, $\epsilon = 0.0418$, $R = 10^6$		
0.01	0	0	0	0	0	0	0	0
0.055	−1.1149	2.04×10^{-4}	159.4	5.31×10^{-4}				
0.10					−0.7851	1.039×10^{-4}	538.9	2.69×10^{-4}
0.155	−1.203	4.25×10^{-4}	333.9	0.001113				
0.2					−0.9089	1.778×10^{-4}	924.7	$4.62 \times 10^{-}$
0.255	−1.218	5.75×10^{-4}	451.2	0.001504				
0.3					−0.9445	2.324×10^{-4}	1209	$6.05 \times 10^{-}$
0.355	−1.224	6.94×10^{-4}	544.8	0.001816				
0.4					−0.9616	2.771×10^{-4}	1442	$7.21 \times 10^{-}$
0.455	−1.228	7.96×10^{-4}	624.8	0.002083				
0.5					−0.9713	3.158×10^{-4}	1644	$8.22 \times 10^{-}$
0.555	−1.230	8.87×10^{-4}	695.8	0.002319				
0.6					−0.9766	3.504×10^{-4}	1824	$9.12 \times 10^{-}$
0.655	−1.230	9.69×10^{-4}	760.2	0.002534				
0.7					−0.9777	3.818×10^{-4}	1987	9.94×10^{-4}
0.755	−1.229	0.001044	819.5	0.002731				
0.8					−0.9715	4.106×10^{-4}	2137	0.001069
0.855	−1.224	0.001114	874.2	0.002914				
0.9					−0.9467	4.362×10^{-4}	2270	0.001135
0.955	−1.204	0.001175	921.5	0.003072				
0.99					−0.8206	4.417×10^{-4}	2293	0.001146
0.995	−1.159	0.001195	936.3	0.003121				

[a] Rough location of the point of instability.

$$\frac{d\Lambda_E}{dx^*} = \frac{1}{f_3(\Lambda_E)} \left\{ \left[\frac{dz^*}{dx^*} \frac{dU_0^*}{dx^*} + z^* \frac{d^2U_0^*}{dx^{*2}} \right] + \frac{1}{U_0^*} \left(Q_0^* \frac{dz^*}{dx^*} + z^* \frac{dQ_0^*}{dx^*} \right) - \frac{1}{U_0^{*2}} \left(Q_0^* z^* \frac{dU_0^*}{dx^*} \right) \right\} \quad (42b)$$

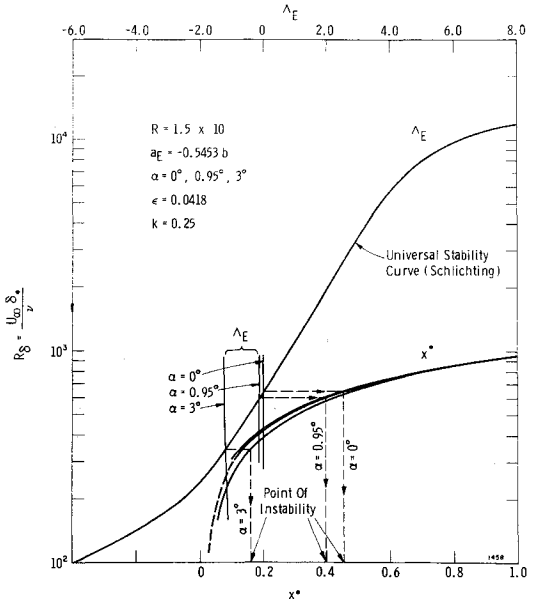

Fig. 4 Determination of the point of instability.

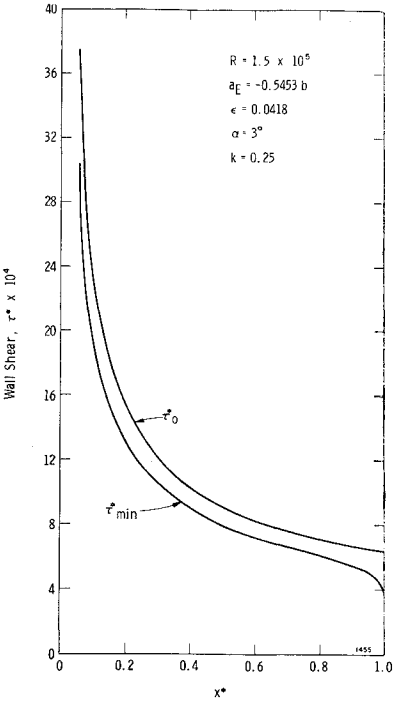

Fig. 5 An example of the wall shears.

Table 3 Effect of the parameter ϵ on the boundary-layer characteristics

	$\alpha_0 = 0.95°$, $\epsilon = 0.02$				$\alpha_0 = 0.95°$, $\epsilon = 0.06$			
x	Λ_E	θ^*	R_δ	$\delta_*{}^*$	Λ_E	θ^*	R_δ	$\delta_*{}^*$
0.01	−0.2165	6.48×10^{-5}	49.8	1.66×10^{-4}	−0.1728	1.245×10^{-4}	95.7	3.19×10^{-4}
0.10	−1.280	3.67×10^{-4}	288.3	9.60×10^{-4}	−0.1629	3.88×10^{-4}	298.5	9.95×10^{-4}
0.20	−1.282	5.35×10^{-4}	420.0	1.400×10^{-3}	−0.1644	5.53×10^{-4}	425.3	1.418×10^{-3}
0.30	−1.282	6.61×10^{-4}	519.6	1.73×10^{-3}	−0.1649	6.78×10^{-4}	522.4	1.741×10^{-3}
0.40	−1.283	7.68×10^{-4}	603.1	2.010×10^{-3}	−0.1653	7.86×10^{-4}	604.2	2.014×10^{-3}
0.50	−1.283	8.61×10^{-4}	676.4	2.255×10^{-3}	−0.1655	8.80×10^{-4}	676.2	2.254×10^{-3}
0.60	−1.283	9.45×10^{-4}	742.4	2.476×10^{-3}	−0.1656	9.64×10^{-4}	741.3	2.471×10^{-3}
0.70	−1.283	1.022×10^{-3}	803.1	2.677×10^{-3}	−0.1656	1.042×10^{-3}	801.0	2.670×10^{-3}
0.80	−1.282	1.094×10^{-3}	859.4	2.865×10^{-3}	−0.1653	1.114×10^{-3}	856.6	2.855×10^{-3}
0.90	−1.282	1.161×10^{-3}	912.2	3.041×10^{-3}	−0.1642	1.182×10^{-3}	908.7	3.029×10^{-3}
0.99	−1.277	1.217×10^{-3}	956.0	3.187×10^{-3}	−0.1591	1.239×10^{-3}	951.9	3.172×10^{-3}

where

$$f_1(\Lambda_E) = \frac{\delta_*{}^*}{\theta^*} = \frac{\frac{3}{10} - \frac{1}{120}\Lambda_E}{\frac{37}{315} - \frac{1}{945}\Lambda_E - \frac{1}{9072}\Lambda_E{}^2} \quad (43a)$$

$$f_2(\Lambda_E) = (2R\tau_0\delta^*/U_0^*)((\theta^*/\delta^*) = (2 + \tfrac{1}{16}\Lambda_E)(\tfrac{37}{315} - \tfrac{1}{945}\Lambda_E - \tfrac{1}{9072}\Lambda_E{}^2) \quad (43b)$$

$$f_3(\Lambda_E) = (dK/d\Lambda_E) = (\tfrac{37}{315} - \tfrac{1}{945}\Lambda_E - \tfrac{1}{9072}\Lambda_E{}^2) \times (\tfrac{37}{315} - \tfrac{1}{315}\Lambda_E - \tfrac{5}{9072}\Lambda_E{}^2) \quad (43c)$$

For general applications to thin foils, $U_0{}^* = 1$ will be used. This may be a conservative estimate in the sense that the leading-edge favorable pressure gradient is neglected, and, thus, the transition and/or separation may be slightly hastened. Then the initial conditions are

$$z^* = 0 \quad (44a)$$

$$\Lambda_E{}^* = 0 \quad (44b)$$

Since $I(x^*)$ in the viscous solution is indeterminate at $x^* = 0$, the integration is started from a small number, say, 0.00001. The separation point of the mean boundary layer occurs at $(\partial u^*/\partial\eta)_{\eta=0} = 0$ or $\Lambda_E = -12$. The point of instability may be determined approximately by the universal stability curve (Fig. 17.3 of Ref. 12) using $\Lambda = \Lambda_E$ and

$$U_\infty\delta_*/\nu = R_\delta = 2R\delta_*{}^* = 2Rf_1(\Lambda_E)\theta^* \quad (45)$$

Presumably, transition takes place near the point of instability. The separation point of the resultant unsteady boundary layer will be defined at present as the location where the minimum wall shear vanishes. The effect of turbulent flow is to delay separation, since flow retardation is decreased because of macroscopic momentum transfer.

Examples

The test model in Fig. 17 of Ref. 5 is taken here as an example. The leading-edge radius is approximately $r_0 = 0.014b$ which yields $\epsilon = 0.0418$ based on Eq. (24). The axis is located at $a_E = -0.5453b$. The Reynolds number R in the test was 1.5×10^5 (or 3.0×10^5 if R is based on chord).

The approximate unsteady potential flow components at the edge of the boundary layer are shown in Fig. 2. The assumption of $d\alpha/dx = 0(\delta)$ seems to be good for $k = 0.25$ but no so good for $k = 1.0$; however, some qualitative answer may still be obtained for $k = 1.0$. The effect of leading-edge curvature is shown in Table 1.

The displacement and momentum thickness for the aforementioned model at $R = 1.5 \times 10^5$, $k = 0.25$, $\alpha_0 = 0.95°$ are given in Fig. 3. The effect of the amplitude of oscillation is given in Table 2, which shows appreciable effect only at the leading edge. The effect of leading-edge curvature is small as given in Table 3. The boundary-layer thicknesses become thinner for higher Reynolds numbers, as shown in Table 4.

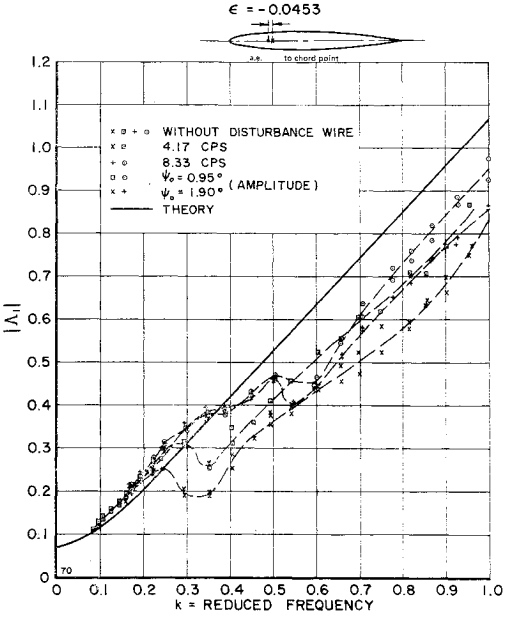

Fig. 6a Influence of amplitude of rotation on magnitude of moment for an aerofoil without disturbance wires.[5]

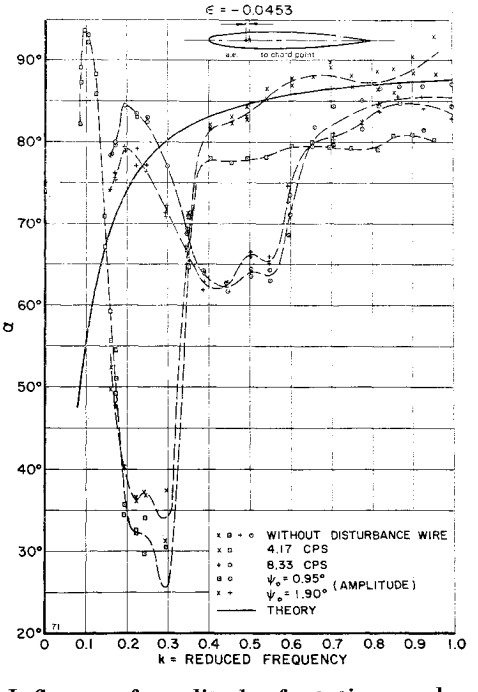

Fig. 6b Influence of amplitude of rotation on phase angle of moment for an aerofoil without disturbance wires.[5]

Table 4 Effect of Reynolds number on boundary-layer characteristics

($\alpha_0 = 3°$, $k = 0.25$, $\epsilon = 0.0418$, $a_E = -0.5453$)

	$R = 10^4$				$R = 10^6$			
x	Λ_E	θ^*	R_δ	$\delta_*{}^*$	Λ_E	θ^*	R_δ	$\delta_*{}^*$
0.01	0	0	0	0	0	0	0	0
0.055	−1.114	7.88×10^{-4}	41.2	0.002058	−1.114	0.789×10^{-4}	412	2.05×10^{-4}
0.10								
0.155	−1.203	0.001649	862.0	0.00431	−1.203	1.648×10^{-4}	862	4.31×10^{-4}
0.20								
0.255	−1.218	0.002272	116.5	0.00582	−1.218	2.227×10^{-4}	1165	5.82×10^{-4}
0.30								
0.355	−1.224	0.002689	140.7	0.00703	−1.224	2.689×10^{-4}	1407	7.03×10^{-4}
0.40								
0.455	−1.228	0.003084	161.3	0.00807	−1.227	3.084×10^{-4}	1613	8.07×10^{-4}
0.50								
0.555	−1.230	0.00343	1797.0	0.00898	−1.230	3.43×10^{-4}	1797	8.98×10^{-4}
0.60								
0.655	−1.230	0.00375	196.3	0.00981	−1.230	3.75×10^{-4}	1963	9.81×10^{-4}
0.70								
0.755	−1.229	0.00404	211.6	0.01058	−1.229	4.04×10^{-4}	2116	0.001058
0.80								
0.855	−1.224	0.00431	225.7	0.01129	−1.224	4.31×10^{-4}	2257	0.001129
0.90								
0.955	−1.204	0.00455	237.9	0.01190	−1.204	4.55×10^{-4}	2379	0.001190
0.99								
0.995	−1.159	0.00463	241.7	0.01209	−1.159	4.63×10^{-4}	2417	0.001209

The locations of the point of instability with $\alpha_0 = 0$, 0.95, and 3° are given in Fig. 4. First, one finds the intersection of R_δ vs Λ_E curve with the universal stability curve. Next, one finds that the location x^* corresponds to the Reynolds number R_δ at the point of instability (from the R_δ vs x^* curve). The location of the point of instability is seen to be sensitive to the amplitude of oscillation.

The wall shear of the mean boundary layer and the minimum wall shear distribution are given in Fig. 5. The effect of the Reynolds number R is given in Table 5. It is seen that nowhere is the wall shear zero. In fact, the unsteady wall shear is only about one-tenth of the mean wall shear. Hence, there appears no point of separation.

Discussion

The discrepancy of theoretical and experimental values of moment without disturbance wire[5] are shown in Fig. 6. It was attributed to the oscillation of the transition point. However, it is difficult to see how the pressure imposed on the boundary layer would be affected by the oscillation of the transition point. The change of the slope of the displacement thickness may be of the order of 10^{-3} which takes place over a range of 0.1 chord. This effect would be small compared with that effect of the oscillation of the foil of 1° over the whole chord. Yet, significant error in prediction by the potential flow was found in Ref. 5 when there was no disturbance wire to trigger turbulence. This may be a challenging problem for future study. However, there is another possible cause of separation due to growth of some unsteady components inside the boundary layer after the point of instability.

Aside from the existence of waves of two-chord lengths, it can be shown from the nonlinear equation (with $u' \partial u'/\partial x$ term, say) that there may exist also waves of four-chord length. For qualitative discussions, the stability curve fo

Table 5 Effect of the Reynolds number of the nondimensional wall shears

	$R = 1.5 \times 10^5$		$R = 1 \times 10^6$		$R = 1 \times 10^4$	
x^*	$\tau_{min}{}^*$	$\tau_0{}^*$	$\tau_{min}{}^*$	$\tau_0{}^*$	$\tau_{min}{}^*$	$\tau_0{}^*$
0.01						
0.055	0.003035	0.003745	0.001175	0.001450	0.01175	0.01450
0.1						
0.155	0.001520	0.001787	5.89×10^{-4}	6.92×10^{-4}	0.00589	0.00692
0.2						
0.255	0.001142	0.001325	4.42×10^{-4}	5.12×10^{-4}	0.00442	0.00512
0.3						
0.355	9.53×10^{-4}	0.001095	3.69×10^{-4}	4.24×10^{-4}	0.00369	0.00424
0.4						
0.455	8.36×10^{-4}	9.55×10^{-4}	3.23×10^{-4}	3.69×10^{-4}	0.00324	0.00370
0.5						
0.555	7.54×10^{-4}	8.57×10^{-4}	2.92×10^{-4}	3.32×10^{-4}	0.00292	0.00332
0.6						
0.655	6.90×10^{-4}	7.85×10^{-4}	2.67×10^{-4}	3.04×10^{-4}	0.00267	0.00304
0.7						
0.755	6.35×10^{-4}	7.28×10^{-4}	2.82×10^{-4}	2.46×10^{-4}	0.00246	0.00282
0.8						
0.855	5.76×10^{-4}	6.82×10^{-4}	2.23×10^{-4}	2.64×10^{-4}	0.00223	0.00264
0.9						
0.955	5.11×10^{-4}	6.48×10^{-4}	1.98×10^{-4}	2.51×10^{-4}	0.00198	0.00250
0.99						
0.995	4.02×10^{-4}	6.38×10^{-4}	1.56×10^{-4}	2.47×10^{-4}	0.00156	0.00247

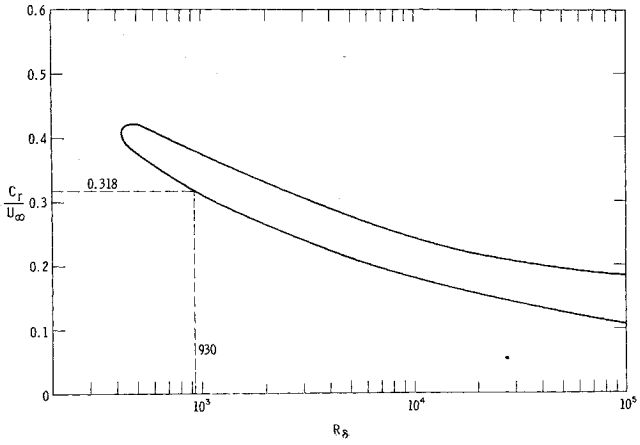

Fig. 7 Curve of neutral stability for the wave propagation velocity C_r.

$\Lambda_E = 0$ (see Fig. 7 and Ref. 12, p. 397) will be employed which shows that the waves of four-chord length at $k = 0.25$, ($\alpha = \pi/2c$, $c_r/u_\infty = \omega/\alpha U_\infty = 1/\pi = 0.318$) becomes unstable at $R_\delta \cong 930$ which occurs near the trailing edge of the foil (Fig. 5). At $k = 0.5$, the waves of four-chord length become stable ($c_r/U_\infty = 0.636$), while the waves of two-chord length ($\alpha = \pi/c$, $c_r/U_\infty = \omega/\alpha U_\infty = 0.318$) become unstable; consequently, large deviation from the classical theory may be possible because of oscillatory separation of the boundary layer. This is a tentative explanation for the discrepancies. It is recommended, therefore, that a flow visualization study (preferably with simultaneous lift and moment measurement) be undertaken so that a definite explanation can be given and methods to prevent the deviation from classical theory can then be devised to facilitate flutter predictions.

Conclusions

For finite but small amplitude oscillations at zero mean incidence, the effective pressure gradient due to unsteady motion does not cause a large change in the boundary-layer characteristics except in the location of the point of instability. The minimum wall shear of the resultant boundary layer does not vanish anywhere on the foil and thus does not seem to produce a separation point. The large deviation in measured motion from classical theory seems to suggest that a new kind of instability of the unsteady waves at the given frequency leads to oscillatory separation. It is not clear how the turbulent growth would interact with this instability. On the other hand, it is also possible that the effect of oscillatory transition point is not negligible. Considerably more work remains to be done for better understanding of the unsteady boundary-layer flow over a pitching and/or heaving foil. Flow visualization studies with the given foil or simultaneous lift and moment measurements are highly recommended for this purpose.

References

[1] Abramson, H. N., Chu, W. H., and Irick, J. T., "Hydroelasticity with Special Reference to Hydrofoil Craft," Monograph for Dept. of Navy, David Taylor Model Basin, Washington, D.C., Aug. 1966, Southwest Research Institute.

[2] Abramson, H. N. and Chu, W. H., "A Discussion of the Flutter of Submerged Hydrofoils," *Journal of Ship Research*, Vol. 3, No. 2, Oct. 1959, pp. 5–13.

[3] Abramson, H. N. and Ransleben, G. E., Jr., "An Experimental Investigation of Flutter of a Fully Submerged Subcavitating Hydrofoil," Tech. Rept. 4, Contract Nonr-3335(00), SwRI Project 38-1028-2, Dec. 1963; also Paper 64-307, 1964, AIAA; also *Journal of Aircraft*, Vol. 2, No. 5, Sept.-Oct. 1965, pp. 439–442.

[4] Chu, W. H., "A Critical Reevaluation of Hydrofoil Theories and Experiments in Subcavitating Hydrofoil Flutter," *Journal of Ship Research*, Vol. 10, No. 2, June 1966.

[5] Greidanus, J. H., Van de Vooren, A. I., and Bergh, H., "Experimental Determination of the Aerodynamic Coefficients of an Oscillating Wing in Incompressible Two-Dimensional Flow: Part I, Wing with Fixed Axis of Rotation," Rept. F 101, 1952, National Aero and Astronautical Research Institute, Amsterdam, Holland.

[6] Moore, F. K., "Unsteady Laminar Boundary Layer Flow," TN2471, 1951, NACA.

[7] Kestin, J., Meader, P. F., and Wang, H. E., "On Boundary Layer Associated with Oscillating Streams," *Applied Scientific Research*, Section A, Vol. 10, 1961.

[8] Lin, C. C., "Motion in the Boundary Layer with a Rapidly Oscillating External Flow," *9th International Congress of Applied Mechanics*, Vol. 4, 1957.

[9] Chu, W. H., "An Aerodynamic Analysis for Flutter in Oseen Type Viscous Flow," *Journal of the Aerospace Sciences*, Vol. 29, No. 7, July 1962, pp. 781–789; see also Chu, W.-H., "Errata: 'An Aerodynamic Analysis for Flutter in Oseen-Type Viscous Flow'," *AIAA Journal*, Vol. 3, No. 8, Aug. 1965, p. 1568.

[10] Crimi, P., "The Effects of Viscosity on the Flow about an Oscillating Flat Plate," Ph.D. thesis, 1964, Aerospace Engineering, Cornell University, 1964 (available from University Microfilm Inc., Ann Arbor, Mich.).

[11] Stewardson, K., "Theory of Unsteady Laminar Boundary Layers," *Advances in Applied Mechanics*, Vol. 6, Academic Press, 1960, pp. 1–37.

[12] Schlichting, H., *Boundary Layer Theory*, translated by J. Kestin, 4th ed., McGraw-Hill, New York, 1962.

[13] Chu, W. H., "Some Contributions to Unsteady Hydrodynamics in Engineering," Ph.D. dissertation, Part III, Sec. 1, June 1963, The Johns Hopkins University, pp. 199–214 (available from University Microfilm Inc., Ann Arbor, Mich.).

[14] Bisplinghoff, R. L., Ashley, H., and Halfman, R. L., *Aeroelasticity*, 2nd printing, Addison-Wesley, 1957.